Available online at www.sciencedirect.com
SCIENCE DIRECT®
Catalysis Today 89 (2004) 183–191
CATALYSIS TODAY
www.elsevier.com/locate/cattod

Partial oxidation of methane to syngas over glow discharge plasma treated Ni–Fe/Al_2O_3 catalyst

Jian-guo Wang [a,b], Chang-jun Liu [a,b,*], Yue-ping Zhang [c], Kai-lu Yu [a,b], Xin-li Zhu [a,b], Fei He [a,b]

[a] *Key Laboratory of Green Chemical Technology, School of Chemical Engineering, Tianjin University, Tianjin 300072, China*
[b] *ABB Plasma Greenhouse Gas Chemistry Laboratory, Tianjin University, Tianjin 300072, China*
[c] *Department of Chemistry, Tianjin University, Tianjin 300072, China*

Abstract

Ni–Fe/Al_2O_3 catalyst for partial oxidation of methane was prepared first by glow discharge plasma treatment following by calcinations thermally. Such prepared catalyst exhibits better performance over the catalyst prepared without such plasma treatment. The conversion of methane and the selectivity of CO and H_2 over the plasma treated catalyst are 97.44, 100 and 100% at 875 °C, while, at the same temperature, they are 90.09, 97.28 and 97.09%, respectively, over the catalyst prepared without plasma treatment. At the same methane conversion, the reaction temperature with the plasma treated Ni–Fe/Al_2O_3 is at least 80 °C lower. TEM characterization shows that the catalytically active species after plasma treatment are still highly dispersed on the support. In addition, the plasma treated Ni–Fe/Al_2O_3 catalyst also possesses better anti-carbon deposit ability.

Keywords: Glow discharge; Plasma; Ni/Al_2O_3; Partial oxidation; Catalyst; Methane; Syngas

1. Introduction

Syngas (a mixture of CO and H_2) is a very important feedstock for the production of many important chemicals, like methanol, ammonia and synthetic fuels [1]. A major syngas production is via the steam reforming of natural gas, with which methane is the principal component [2]. However, there exist several disadvantages with the steam reforming, like high-energy consumption and high H_2/CO ratio. Partial oxidation of methane to syngas is a very promising alternative to the steam reforming [3,4]. A great effort has been given to the partial oxidation methane for the syngas production. Some progresses have been achieved [4]. The catalysts investigated are mainly the transition metal (Ni, Co and Fe) [5,6] and the noble metal (Ru, Rh, Pd, Pt and Ir) supported catalysts [7–11]. Among these catalysts, nickel-based catalysts, such as Ni/Al_2O_3 [12–15], NiO–MgO [16–18], and NiO–rare earth oxides [19,20], show high activity and selectivity with low cost. In practice, Ni-based catalysts are more promising than noble metal catalysts. However, the reaction with the nickel-based catalysts starts only at high temperature [21], and coke deposition on nickel is much faster than that on noble metals [22]. Therefore, the development of coking-resistant Ni-based catalyst with lower temperature activity is very important for the future application of partial oxidation of methane for syngas production.

Previous investigations have found that the highly dispersed nano-structured catalyst can inhibit the coke formation and present a better activity [23,24]. It has been reported that thermal plasma can be used for the production of highly dispersed catalysts [25]. Vissokov and Panayotova applied plasma synthesis and regeneration of catalyst for reforming of methane [26]. Zhang et al. also reported a radio frequency plasma treatment for Ni-Al_2O_3 catalyst [27] and a 3–5% higher methane conversion has been achieved. In this work, we attempt to use a glow discharge treatment following by calcinations thermally to produce the highly dispersed nano-structured Ni–Fe/Al_2O_3 catalyst for a better syngas production via partial oxidation of methane. Glow discharge is a non-thermal plasma phenomenon. Different from the thermal plasma [26] and from the plasma used for the activation of catalyst [27], the glow discharge operates at room temperature and low pressure. Highly energetic

* Corresponding author. Fax: +86-22-27890078.
E-mail address: changliu@public.tpt.tj.cn (C.-j. Liu).

0920-5861/$ – see front matter © 2003 Elsevier B.V. All rights reserved.
doi:10.1016/j.cattod.2003.11.025

electrons normally characterize most regions of glow discharge [25] and induce a lot of unusual phenomena.

2. Experimental

2.1. Catalyst preparation

The conventional wetness impregnation has been applied for the preparation of Ni–Fe/Al_2O_3 catalyst (Ni:Fe:Al_2O_3 = 7:3:90 (wt.)). The Al_2O_3 powder support was first impregnated in an aqueous solution of $Ni(NO_3)_2$ and $Fe(NO_3)_3$ for ca. 6 h at room temperature. After impregnation, the obtained sample was then divided into two parts: one for calcinations at 600 °C for 6 h after drying at 90 °C for 16 h, and the other for plasma treatment at room temperature for only 1 h before further calcinations at 600 °C for 6 h. In this work, we have successfully utilized a dc glow discharge for plasma treatment of catalyst. The electrode configuration of plasma is the same with the previous literature (Fig. 1(a) in [25]). The catalyst was located in the "positive column" of glow discharge [25] that was generated at ca. 12 Pa and at room temperature using argon as the glow discharge plasma-forming gas. The treatment time was ca. 1 h.

2.2. Partial oxidation of methane to syngas

The catalyst was pressed, crushed and sieved to 40–60 meshes before test. The catalyst was then placed in a 6 mm i.d. quartz tube flow reactor. The catalyst weight is 40 mg. The schematic diagram of the setup used for the partial oxidation is shown in Fig. 1. Before reaction, the catalyst was reduced in a flowing hydrogen for 1 h at 650 with the flow rate of 50 cm^3/min. The reaction temperature was measured by a thermocouple attaching directly to the catalyst bed. The feed was a mixture of methane and oxygen (CH_4:O_2 = 2:1). The feed and the product gases were analyzed by an on-line gas chromatograph (Agilent 4890) using a thermal conductivity detector (TCD) with a TDX-01 column.

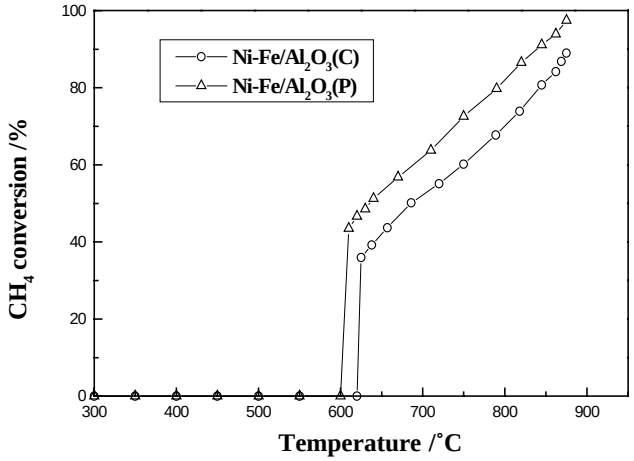

Fig. 2. Effect of the reaction temperature on CH_4 conversion. Reaction conditions: Ni:Fe:Al_2O_3 = 7:3:90 (wt.), P = 1 atm, GHSV = 90 000 cm^3/g h, CH_4/O_2 = 2.

2.3. Catalyst characterization

The surface area of catalysts applied was determined by nitrogen adsorption using a CHEMBET3000 apparatus. The morphology of the fresh and used catalysts was observed with a JEOL JEM-100CX II transmission electron microscope (TEM). The X-ray diffraction (XRD) characterization was conducted using a D-MAX-2500X-R diffractometer (Cu Kα, 40 kV, 100 mA). X-ray photoelectron spectroscopy (XPS) studies were performed using a PHI1600 XPS system with Al Kα radiation.

3. Results and discussion

3.1. Catalyst activity and selectivity

The catalytic tests were performed with a temperature range from 300 to 875 °C. The effect of the reaction temperature on the conversion of methane is shown in Fig. 2. In the following discussions, the catalyst prepared without

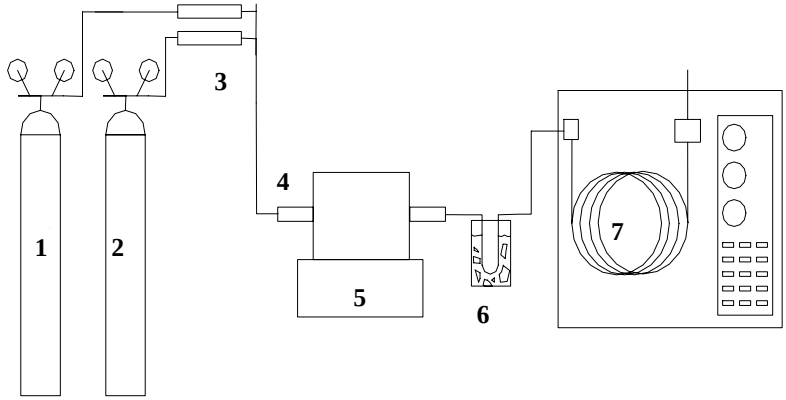

Fig. 1. Schematic diagram of the equipment used for partial oxidation of methane: 1, CH_4 cylinder; 2, oxygen cylinder; 3, mass flow controllers; 4, reactor; 5, furnace; 6, ice trap; 7, GC.

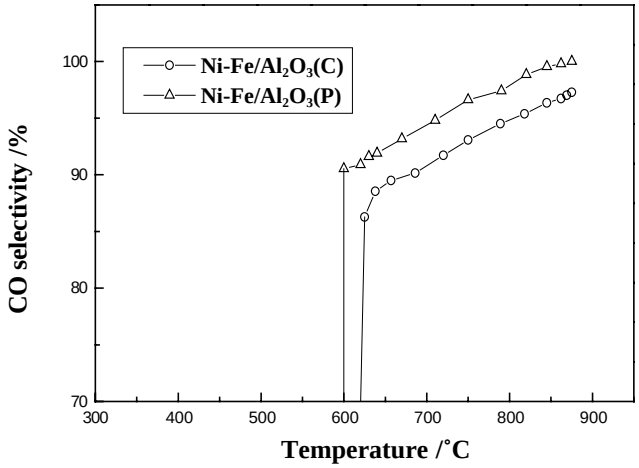

Fig. 3. Effect of the reaction temperature on CO selectivity. Reaction conditions: Ni:Fe:Al_2O_3 = 7:3:90 (wt.), P = 1 atm, GHSV = 90 000 $cm^3/g\,h$, CH_4/O_2 = 2.

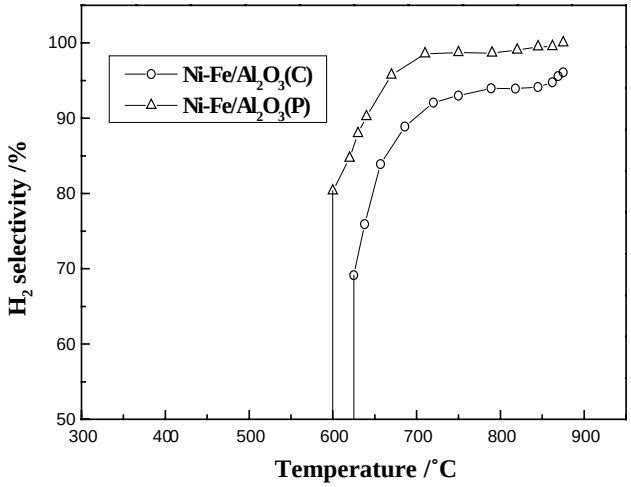

Fig. 4. Effect of the reaction temperature on H_2 selectivity. Reaction conditions: Ni:Fe:Al_2O_3 = 7:3:90 (wt.), P = 1 atm, GHSV = 90 000 $cm^3/g\,h$, CH_4/O_2 = 2.

plasma treatment is referred to as Ni–Fe/Al_2O_3(C), and the plasma treated catalyst is referred to as Ni–Fe/Al_2O_3(P).

Fig. 2 shows Ni–Fe/Al_2O_3(P) is more active than Ni–Fe/Al_2O_3(C). The reaction initiative temperature (T_i) for Ni–Fe/Al_2O_3(P) was 600 °C, 25 °C lower than that with Ni–Fe/Al_2O_3(C). The syngas production from partial oxidation of methane over the reported conventional Ni/Al_2O_3 catalyst started at ca. 750 °C [21]. Ni–Fe/Al_2O_3(P) shows a much better low temperature activity. The methane conversion for Ni–Fe/Al_2O_3(P) catalyst within this temperature range is 6–12% higher than that obtained over the conventional catalyst. At the same methane conversion, the reaction temperature with Ni–Fe/Al_2O_3(P) is at least 80 °C lower than that with Ni–Fe/Al_2O_3(C).

The effect of temperature on the selectivity of CO and H_2 is shown in Figs. 3 and 4. In the temperature range discussed, the selectivity of CO is 90.53–100% over Ni–Fe/Al_2O_3(P), which is 3–7% higher than that over Ni–Fe/Al_2O_3(C). The selectivity of H_2 over Ni–Fe/Al_2O_3(P) is more than 95% at the temperature higher than 700 °C. At 875 °C, the selectivity of both CO and H_2 reaches 100%. The H_2/CO ratio of syngas over Ni–Fe/Al_2O_3(P) is ca. 2, which is very suitable for further Fisher–Tropsch synthesis or methanol synthesis. The selectivity of H_2 over Ni–Fe/Al_2O_3(C) is 5–8% lower than that over Ni–Fe/Al_2O_3(P). Oxygen is completely consumed for both catalysts. The methane conversion and the selectivity of CO and H_2 over Ni–Fe/Al_2O_3(P) are 97.44, 100 and 100%, respectively, at 875 °C. At the same temperature, the methane conversion and the selectivity of CO and H_2 over Ni–Fe/Al_2O_3(C) are 90.09, 97.28 and 97.09%, respectively.

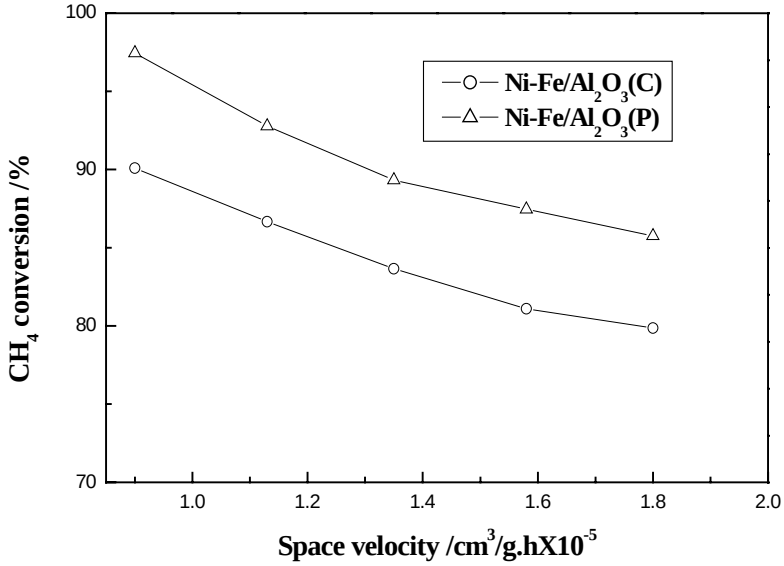

Fig. 5. Effect of space velocity on CH_4 conversion. Reaction conditions: Ni:Fe:Al_2O_3 = 7:3:90 (wt.), P = 1 atm, T = 875 °C, CH_4/O_2 = 2.

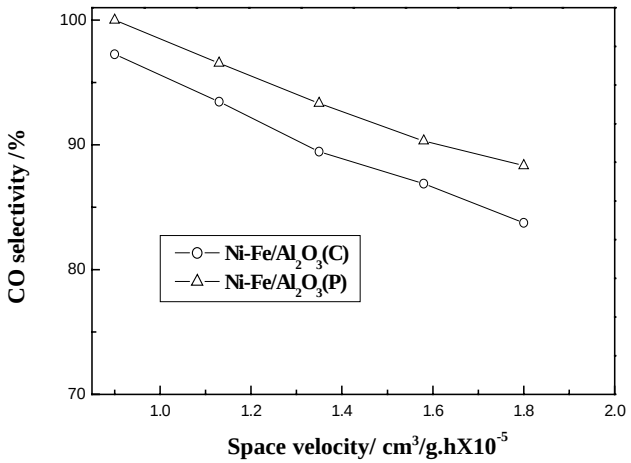

Fig. 6. Effect of space velocity on CO selectivity. Reaction conditions: Ni:Fe:Al_2O_3 = 7:3:90 (wt.), $P = 1$ atm, $T = 875\,^{\circ}C$, $CH_4/O_2 = 2$.

The effect of space velocity on reaction was also investigated at 875 °C. Figs. 5 and 6 were shown the change of methane conversion and CO selectivity with the space velocity. With increasing in space velocity, the activity and selectivity decreased for both catalysts.

3.2. Catalyst characterization

The experimental investigation has shown Ni–Fe/Al_2O_3(P) presents a better activity and selectivity than Ni–Fe/Al_2O_3(C). To understand such plasma-enhanced activity, catalyst characterization has been conducted as discussed below.

3.2.1. Plasma treatment effect on catalyst surface area

From the BET analyses, the surface area of the fresh Ni–Fe/Al_2O_3(C) and the fresh Ni–Fe/Al_2O_3(P) is 156.21 and 136.21 m^2/g, respectively.

Table 1
Comparison of surface atomic compositions from XPS analysis

Atom	Atomic ratio (%)			
	Ni–Fe/Al_2O_3(C)		Ni–Fe/Al_2O_3(P)	
	Fresh	Used	Fresh	Used
O 1s	62.0	48.1	60.7	54.8
Na 1s	0.4	1.0	0.4	0.8
Fe 2p	1.6	0.8	1.2	1.1
Al 2p	26.2	22.5	26.1	26.8
Ni 2p	3.8	1.3	4.4	1.5
C 1s	6.1	26.4	7.1	15.0

3.2.2. XPS study

Table 1 showed the surface compositions for the fresh and used Ni–Fe/Al_2O_3(C) and Ni–Fe/Al_2O_3(P) catalysts. For two kinds of fresh catalysts, carbon content is almost the same. But after reaction, a sharp increase in the carbon content for the Ni–Fe/Al_2O_3(C) is observed when comparing to Ni–Fe/Al_2O_3(P). The increased carbon amount for Ni–Fe/Al_2O_3(C) is 2.5 times higher than that for Ni–Fe/Al_2O_3(P).

The XPS spectra of the fresh Ni–Fe/Al_2O_3(C) and Ni–Fe/Al_2O_3(P) catalysts in C 1s region are showed in Figs. 7 and 8. For two fresh catalysts, the prominent peaks are both at a binding energy of ~284.6 eV in the spectra, which are attributed to the adventitious carbon. The other two small peaks at a binding energy of 286.5 and 288.60 eV may be from some adventitious carbonaceous species and the residual CO_3^{2-}. Figs. 9 and 10 show the XPS spectra of the used Ni–Fe/Al_2O_3(C) and Ni–Fe/Al_2O_3(P) in C 1s region, respectively. After reaction, a small peak appears at binding energy of 282.8 eV on the used Ni–Fe/Al_2O_3(P), which should be assigned to graphitic carbon. But for the used Ni–Fe/Al_2O_3(C), two new and very prominent

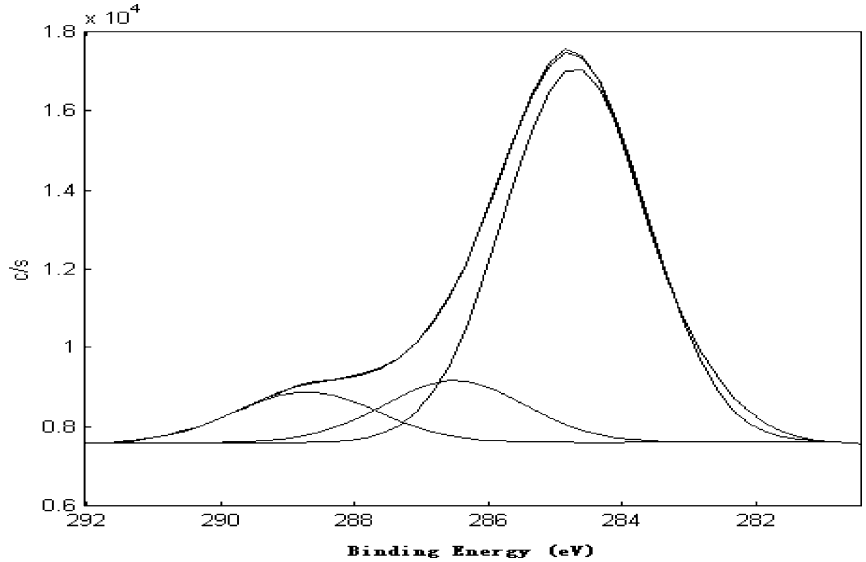

Fig. 7. XPS spectra of fresh Ni–Fe/Al_2O_3(C) in C 1s region.

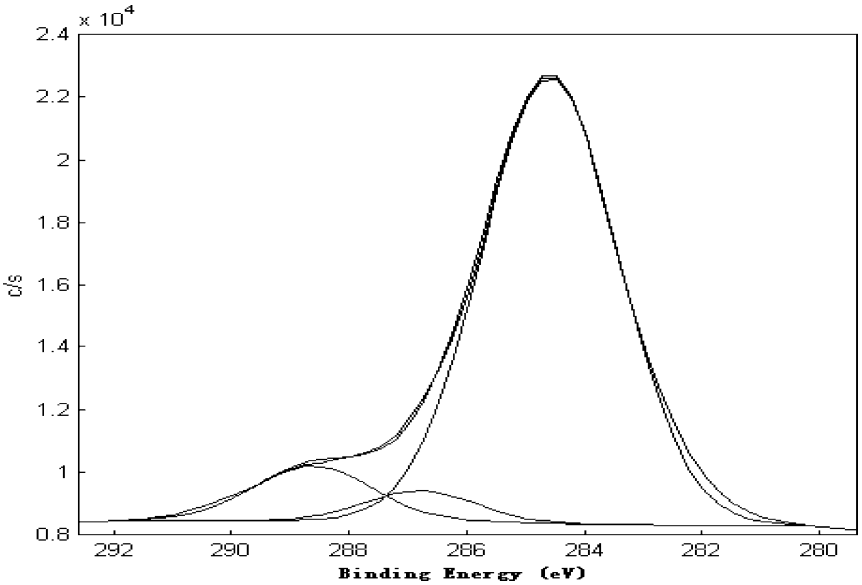

Fig. 8. XPS spectra of fresh Ni–Fe/Al_2O_3(P) in C 1s region.

peaks appeared at binding energy of 280.6 and 282.4 eV. They should be attributed to the metal carbide species and graphitic carbon. And these two kinds of carbon species take 75% in the amount of all carbon species on the used Ni–Fe/Al_2O_3(C), while the amount of the graphitic carbon are about 32% and no metal carbide species were formed with the used Ni–Fe/Al_2O_3(P). Obviously Ni–Fe/Al_2O_3(P) has better anti-carbon deposit ability than Ni–Fe/Al_2O_3(C).

The Ni 2p spectra of the fresh Ni–Fe/Al_2O_3(C) and Ni–Fe/Al_2O_3(P) are present in Fig. 11. In the near-surface region of the fresh catalysts, Ni was characteristic of $NiAl_2O_4$, which is shown by the Ni $2p_{3/2}$ peak at the binding energy of ~856 eV, with an accompanying shake-up satellite peak at ~862 eV [28,29]. The intensity of $NiAl_2O_4$ peak for the Ni–Fe/Al_2O_3(P) was slightly higher than that for Ni–Fe/Al_2O_3(C). The Ni 2p spectra of the used Ni–Fe/Al_2O_3(C) and Ni–Fe/Al_2O_3(P) are shown in Fig. 12. After reaction, metal Ni presents, characterized by a Ni $2p_{3/2}$ peak at a binding energy ~854.5 eV. The intensity of the satellite peak is reduced [29,30]. The metal Ni has been considered as the active component for partial oxidation of methane [31–34]. From Fig. 12, it can be also seen that the intensity of metal Ni for Ni–Fe/Al_2O_3(P) is much higher than that for Ni–Fe/Al_2O_3(C). It could explain that

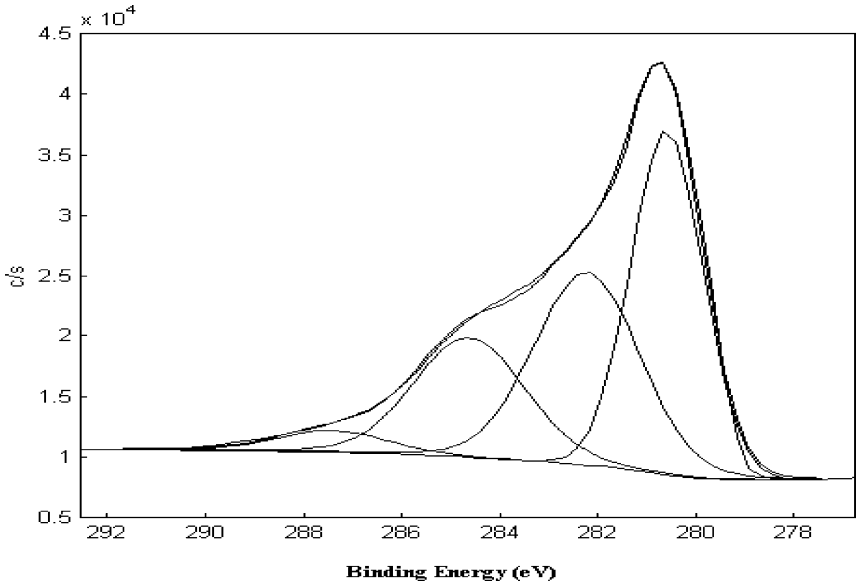

Fig. 9. XPS spectra of used Ni–Fe/Al_2O_3(C) in C 1s region. Reaction conditions: Ni:Fe:Al_2O_3 = 7:3:90 (wt.), P = 1 atm, GHSV = 90 000 $cm^3/g\,h$, CH_4/O_2 = 2, reaction time = 9 h.

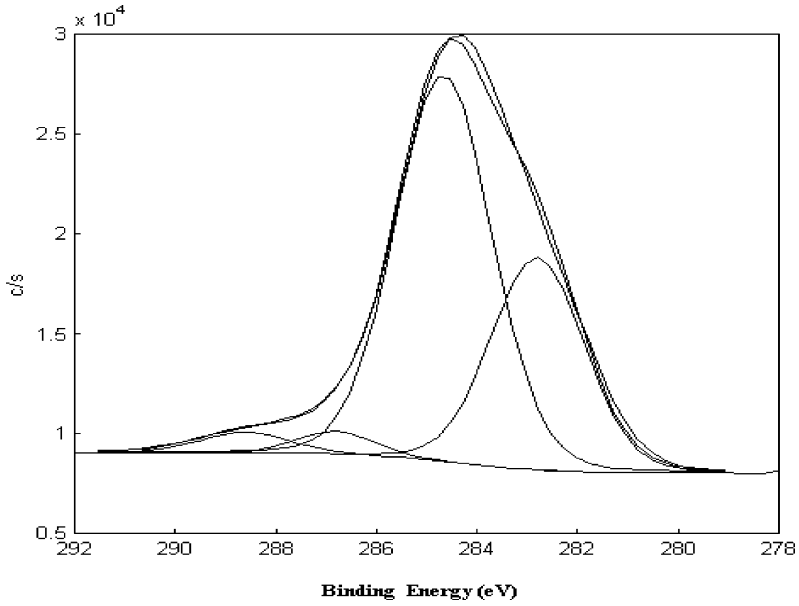

Fig. 10. XPS spectra of used Ni–Fe/Al_2O_3(P) in C 1s region. Reaction conditions: Ni:Fe:Al_2O_3 = 7:3:90 (wt.), P = 1 atm, GHSV = 90 000 cm^3/g h, CH_4/O_2 = 2, reaction time = 9 h.

the activity and selectivity of Ni–Fe/Al_2O_3(P) is better than those of Ni–Fe/Al_2O_3(C).

3.2.3. TEM characterization

Figs. 13 and 14 present the TEM images of the fresh and used Ni–Fe/Al_2O_3(C) and Ni–Fe/Al_2O_3(P) catalysts. Catalytically active species (Ni) with a size in the range of 4–10 nm are highly dispersed on the support for Ni–Fe/Al_2O_3(P). For Ni–Fe/Al_2O_3(C), some big aggregates are observed and the distribution of active species is not uniform. After reaction, a serious carbon deposit is observed on the catalyst Ni–Fe/Al_2O_3(C), as shown in Fig. 13. In addition, the active species in Ni–Fe/Al_2O_3(C) tends to aggregate during reaction. However, the TEM characterization suggests too that the catalyst Ni–Fe/Al_2O_3(P) possesses an excellent anti-carbon deposit performance. As shown in Fig. 14, the active species of Ni–Fe/Al_2O_3(P) is just a little aggregated. Most active species are still highly dispersed on the support. The reason may be attributed to the interaction of active plasma species (a great amount of electrons, radicals, ions, and so on) with the catalyst. In the preparation process, we often treat several times to the same sample. So the catalytic active species (Ni) can be distributed more uniform when compared to the catalyst

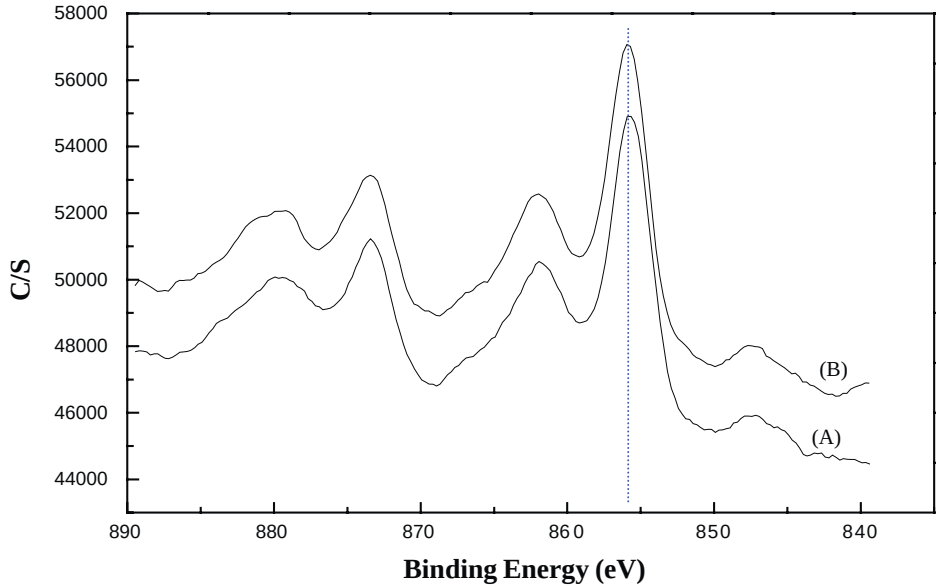

Fig. 11. XPS spectra of fresh catalysts in Ni 2p region: (A) Ni–Fe/Al_2O_3(C); (B) Ni–Fe/Al_2O_3(P).

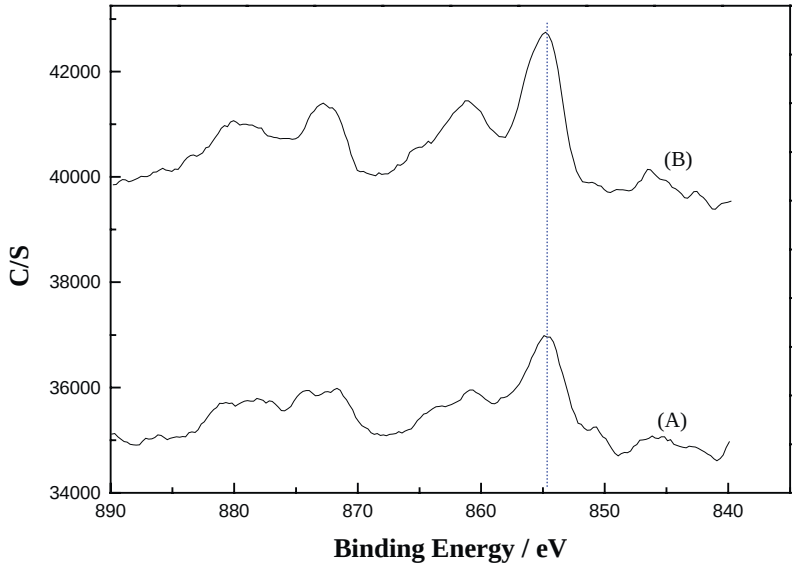

Fig. 12. XPS spectra of used catalysts in Ni 2p region: (A) Ni–Fe/Al_2O_3(C); (B) Ni–Fe/Al_2O_3(P). Reaction conditions: Ni:Fe:Al_2O_3 = 7:3:90 (wt.), P = 1 atm, GHSV = 90 000 cm^3/g h, CH_4/O_2 = 2, reaction time = 9 h.

prepared without plasma treatment. And the addition of Fe can also stabilize the active nickel species [24]. Therefore, the carbon deposit can sharply decrease due to the uniform distribution of active species and the uniform particle distribution.

3.2.4. XRD characterization

XRD diagram of the fresh and hydrogen reduced Ni–Fe/Al_2O_3(C) and Ni–Fe/Al_2O_3(P) was shown in Fig. 15. For the fresh Ni–Fe/Al_2O_3(C) catalysts, the identifiable phases were γ-Al_2O_3 and $NiAl_2O_4$. After reduction using hydrogen, the results of the XRD patterns show that the appearance zero-valent Ni metal besides the γ-Al_2O_3 and $NiAl_2O_4$, which also confirmed that zero-valent Ni metal was responsible for partial oxidation methane to syngas. It is consistent with the XPS results. Comparing to the Ni–Fe/Al_2O_3(C), Ni–Fe/Al_2O_3(P) catalysts did not show the peak with d = 4.4505 ($NiAl_2O_4$). Evidently, the Ni

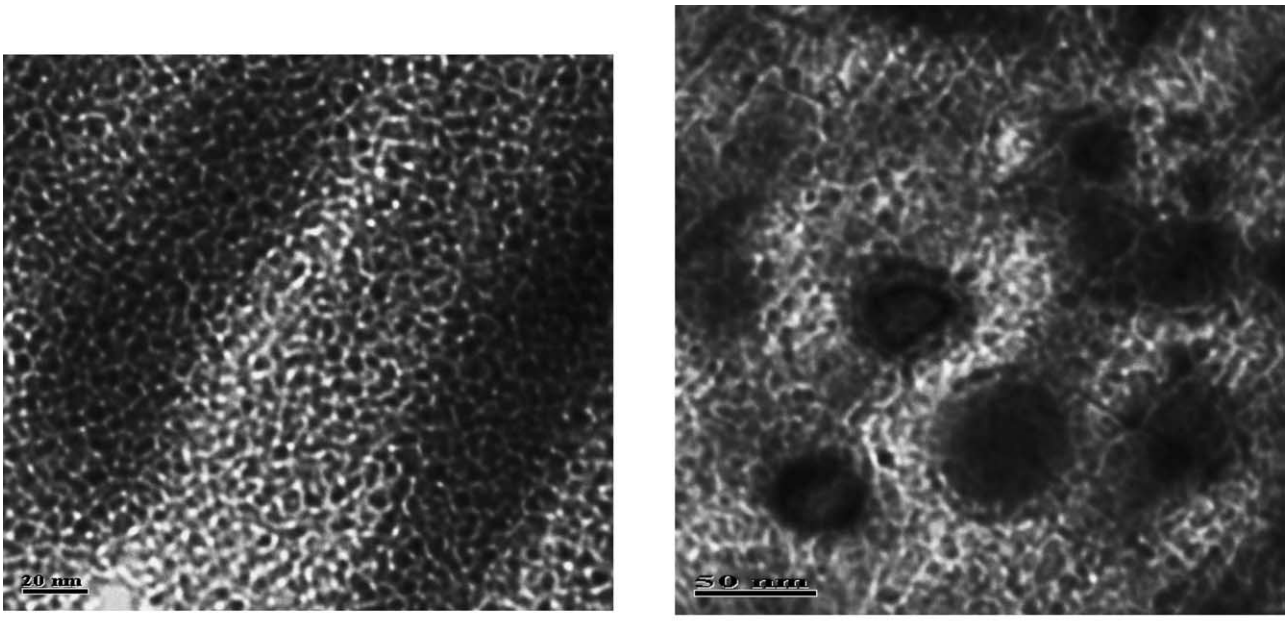

(a) fresh Ni-Fe/Al_2O_3(C) catalyst (b) used Ni-Fe/Al_2O_3(C) catalyst

Fig. 13. TEM images of Ni–Fe/Al_2O_3(C). Reaction conditions: Ni:Fe:Al_2O_3 = 7:3:90 (wt.), P = 1 atm, GHSV = 90 000 cm^3/g h, CH_4/O_2 = 2, reaction time = 9 h.

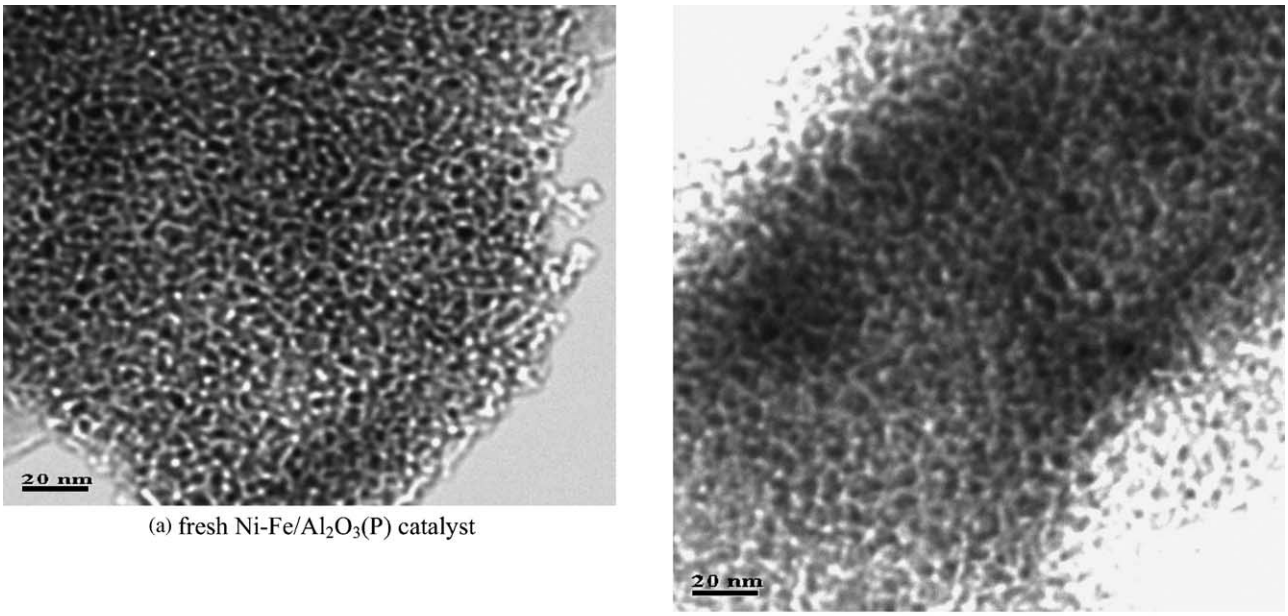

(a) fresh Ni-Fe/Al_2O_3(P) catalyst

(b) used Ni-Fe/Al_2O_3(P) catalyst

Fig. 14. TEM images of Ni–Fe/Al_2O_3(P). Reaction conditions: Ni:Fe:Al_2O_3 = 7:3:90 (wt.), P = 1 atm, GHSV = 90 000 cm^3/g h, CH_4/O_2 = 2, reaction time = 9 h.

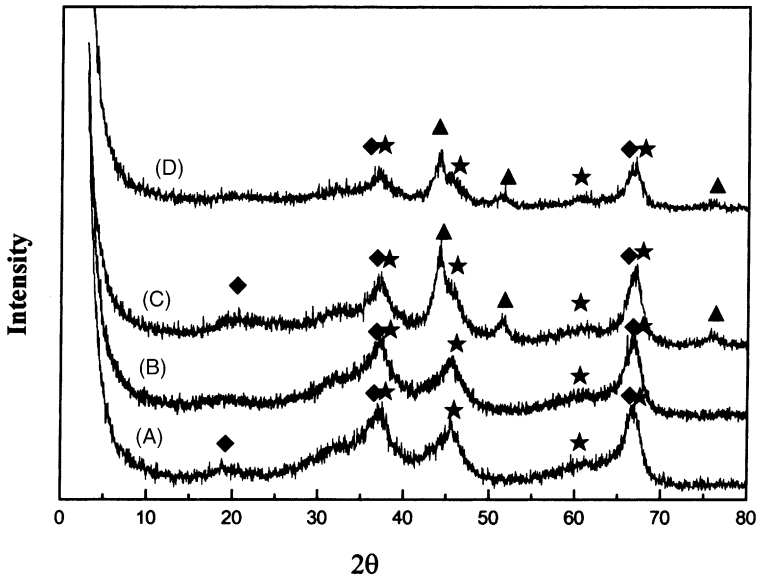

Fig. 15. XRD patterns: (A) fresh Ni–Fe/Al_2O_3(C); (B) fresh Ni–Fe/Al_2O_3(P); (C) reduced Ni–Fe/Al_2O_3(C); (D) reduced Ni–Fe/Al_2O_3(P). (◆) $NiAl_2O_4$; (★) γ-Al_2O_3; (▲) Ni.

species are different over the catalysts prepared in different ways. The plasma treatment would lead to a production of more active Ni species.

4. Conclusions

The present investigation confirms the glow discharge treatment of Ni–Fe/Al_2O_3 catalyst, following by calcinations thermally, leads to a preparation of catalyst with better activity and selectivity for partial oxidation of methane to syngas. The catalyst characterization using XPS and XRD confirms that the discharge treatment induces a better generation of active Ni species. The conversion of methane and the selectivity of CO and H_2 over the plasma treated catalyst are 97.44, 100 and 100% at 875 °C, while, at the same temperature, they are 90.09, 97.28 and 97.09%, respectively. At the same methane conversion, the reaction temperature with the plasma treated Ni–Fe/Al_2O_3 is at least 80 °C lower than that with the conventional Ni–Fe/Al_2O_3. And the plasma

treated Ni–Fe/Al_2O_3 has better anti-carbon deposit ability than Ni–Fe/Al_2O_3(C) does.

Acknowledgements

The authors are grateful for supports from the Major Research Foundation of the Ministry of Education of China (under contract #Major 0212) and ABB Switzerland Ltd.

References

[1] J.R. Anderson, Appl. Catal. 47 (1989) 177.
[2] J.S.-J. Renesme, Y. Muller, Catal. Today 13 (1992) 371.
[3] M.A. Pena, J.P. Gomez, J.L.G. Fierro, Appl. Catal. A 144 (1996) 7.
[4] S.C. Tsang, J.B. Claridge, M.L.H. Green, Catal. Today 23 (1995) 3.
[5] W.J.M. Vermeiren, E. Blomsma, P.A. Jacobs, Catal. Today 13 (1992) 427.
[6] H.Y. Wang, E. Ruckenstein, J. Catal. 199 (2001) 309.
[7] A.T. Ashcroft, A.K. Cheethan, J.S. Ford, M.L.H. Green, C.P. Grey, A.J. Murrel, P.D.F. Vernon, Nature 344 (1990) 319.
[8] C. Elmasides, D.I. Kondarides, S.G. Neophytides, X.E. Verykios, J. Catal. 198 (2001) 195.
[9] R.H. Jones, A.T. Aschcroft, D. Waller, A.K. Cheetham, J.M. Thomas, Catal. Lett. 8 (1991) 169.
[10] D.A. Hichman, L.D. Schmidt, Science 259 (1993) 343.
[11] P.M. Tormiainen, X. Chu, L.D. Schmidt, J. Catal. 146 (1994) 1.
[12] Y. Lu, J. Xue, C. Yu, Y. Liu, S. Shen, Appl. Catal. A 174 (1998) 121.
[13] Q. Miao, G. Xing, S. Sheng, W. Cui, L. Xu, X. Guo, Appl. Catal. A 154 (1997) 17.
[14] L. Cao, Y. Chen, W. Li, Stud. Surf. Sci. Catal. 107 (1997) 467.
[15] Q.G. Yan, W. Chu, L.Z. Gao, Z.L. Yu, S.Y. Yuan, Stud. Surf. Sci. Catal. 119 (1998) 855.
[16] V.R. Choudhary, B.S. Uphade, A.S. Mamman, J. Catal. 172 (1997) 281.
[17] E. Ruckenstein, Y.H. Hu, Appl. Catal. A 183 (1999) 85.
[18] S. Tang, J. Lin, K.L. Tan, Catal. Lett. 51 (1998) 169.
[19] V.R. Choudhary, A.M. Rajput, V.H. Rane, J. Phys. Chem. 96 (1992) 8686.
[20] V.R. Choudhary, V.H. Rane, A.M. Rajput, Catal. Lett. 22 (1993) 289.
[21] V.R. Choudhary, B. Prabhakar, A.M. Rajput, J. Catal. 157 (1995) 752.
[22] J.B. Claridge, M.L.H. Green, S.C. Tsang, Catal. Lett. 22 (1993) 299.
[23] T. Zhu, S.M. Flyzani, Appl. Catal. A 208 (2001) 403.
[24] H. Provendier, C. Perit, C. Estournès, S. Libs, A. Kiennemann, Appl. Catal. A 180 (1999) 163.
[25] C.J. Liu, G.P. Vissokov, B. Jang, Catal. Today 72 (2002) 173.
[26] G.P. Vissokov, M.I. Panayotova, Catal. Today 72 (2002) 213.
[27] Y. Zhang, W. Chu, W. Cao, C. Luo, X. Wen, K. Zhou, Plasma Chem. Plasma Process. 20 (2000) 137.
[28] G.R. Gavalas, C. Phichitkul, G.E. Voecks, J. Catal. 88 (1984) 54.
[29] K.T. Ng, D.M. Hercules, J. Phys. Chem. 80 (1976) 2094.
[30] N.S. McIntyre, T.E. Rummery, M.G. Cook, D. Owen, J. Electrochem. Soc. 123 (1976) 1164.
[31] D. Dhammike, P.R. Michael, C.C.K. Karl, H.L. Jack, J. Catal. 132 (1991) 117.
[32] M.A. Goula, A.A. Lemonidou, W. Grünert, M. Baerns, Catal. Today 32 (1996) 149.
[33] C.T. Au, H.Y. Wang, J. Catal. 167 (1997) 337.
[34] F. van Looij, J.W. Geus, J. Catal. 168 (1997) 154.